



Oligocene-early Miocene paradox of $p\text{CO}_2$ inferred from alkenone carbon isotopic fractionation and sea surface temperature trends

José Guitián^{1*}, Samuel Phelps^{2,3}, Reto S. Wijker¹, Pratiya J Polissar^{2,4}, Laura Arnold¹, and Heather M. Stoll¹

¹Geological Institute, ETH Zurich, Switzerland

²Lamont-Doherty Earth Observatory, Columbia University, USA

³Harvard University, USA

⁴Ocean Sciences Department, University of California Santa Cruz, USA

* *present address*: Centro de Investigación Mariña, Universidade de Vigo, GEOMA, Vigo, 36310, Spain

Correspondence to: Jose Guitian (jose.guitian@uvigo.gal; heather.stoll@eaps.ethz.ch)

Abstract. Atmospheric carbon dioxide decline is hypothesized to drive the progressive cooling over the Cenozoic. However, at multimillion-year timescales during the Oligocene to Miocene time interval the existing reconstructions, most based on the phytoplankton carbon isotopic fractionation (ϵ_p) proxy, differ from what is expected to drive the climate observations.

Here, we produce two new long-term records of ϵ_p over the Oligocene to early Miocene time interval from widely separated locations at IODP Site 1406 and ODP 1168 and increase the resolution of determinations at the equatorial Atlantic ODP 925. These new results confirm a global footprint of ϵ_p shift occurring during this interval. Abrupt 3 ‰ declines are found from 27 to 24.5 Ma and 24 to 22.5 Ma, and minimum ϵ_p is attained at 19 Ma. Between 28.7 and 29.7 Ma at IODP 1406, a higher resolution sampling reveals orbital scale 100 kyr cyclicity in ϵ_p . Making use of alkenone-based sea surface temperature (SST) estimates and benthic $\delta^{18}\text{O}$ estimated extracted from the same samples, we perform a direct comparison with ϵ_p to evaluate the relationship with climate dynamics. We observe that across the long Oligocene to early Miocene interval the two sites' relationships contrast with what is expected if CO_2 was the main driver of ϵ_p and average earth surface temperature evolution was registered at the local surface SST and global benthic $\delta^{18}\text{O}$. Moreover, at orbital timescale, ϵ_p and benthic $\delta^{18}\text{O}$ appear to follow an inverse relationship, although located within the multimillion-year period with the strongest direct correlation between these variables (>25.5 Ma). To evaluate the physiological, non- CO_2 influences on ϵ_p , we use modern cultures to evaluate the impact of changing cell size and growth rate on the trends in ϵ_p . Although at specific time intervals, those drivers seem to explain part of the ϵ_p divergence with SST or benthic $\delta^{18}\text{O}$, most periods remain largely divergent, particularly the late Oligocene warming. We infer that a common CO_2 forcing is likely the dominant control on the coherent temporal trends in ϵ_p at widely separated sites, which experienced contrasting temperature evolution and likely experienced different variations in nutrient availability. While CO_2 changes likely caused significant changes in radiative forcing, SST variation at the examined sites may have been conditioned by regional heat transport, and the relationship between benthic $\delta^{18}\text{O}$ and ϵ_p could reflect variable phasing between ice growth and global temperature.

Short summary. We reconstructed from sediments of different ocean sites phytoplankton carbon isotopic fractionation (ϵ_p), mainly linked to CO_2 variations, during the Oligocene to early Miocene. Records confirm long-term trends but show contrasting relationships with the sea surface temperatures evolution. We evaluate the role of non- CO_2 physiological factors such as temperature and nutrients at each site ϵ_p , highlighting the complexity of interpreting climate dynamics and CO_2 reconstructions.



1 Introduction

Geological records provide key context to current assessments of the consequences of rising atmospheric CO₂ on ice sheet stability and oceanic temperatures (Foster et al., 2017; Golledge, 2020; Zachos et al., 2008). The Oligocene to Miocene time interval has been proposed to represent a nonlinear transition between the ‘greenhouse’ and ‘icehouse’ stages of Earth history (Miller et al., 1991; Zachos et al., 2001) useful to evaluate the Earth system climate sensitivity to the hypothesized progressive CO₂ drawdown of the Cenozoic (Deconto et al., 2008; Zhang et al., 2013). However, the long term decline in CO₂ estimated by existing proxy records contrasts with the rather stable climatic state with multimillion year warming and cooling trends defined by the temperature trends in the deep ocean (Cramer et al., 2011; Lear et al., 2000), and surface ocean (Gutián et al., 2019; Liu et al., 2009; O’Brien et al., 2020) and with estimated Antarctic Ice sheet volume and sea level (Lear et al., 2004; Liebrand et al., 2017; Miller et al., 2020).

Most of the Oligocene and early Miocene *p*CO₂ estimates are derived from the sensitivity of marine algae to CO₂ (Henderiks and Pagani, 2008; Pagani et al., 1999, 2000; Pagani et al., 2005; Super et al., 2018; Zhang et al., 2013) based on the carbon isotopic fractionation in organic matter during photosynthesis (ϵ_p) of marine phytoplankton (Rau et al., 1996), typically measured in biomarkers from haptophyte algae. This fractionation can be reconstructed in the past from sediments by the analysis of $\delta^{13}\text{C}$ of the organic lipids and reconstruction of the $\delta^{13}\text{C}$ of the DIC in the seawater from which biomass was produced. Fractionation (ϵ_p) is predicted to be higher when CO₂ availability is high relative to cellular carbon demand. A decrease in atmospheric CO₂ and consequently in CO₂ of the surface ocean should therefore lead to a decrease in ϵ_p globally. However, in addition to CO₂, the ϵ_p in phytoplankton is affected by physiological factors such as the rate of carbon fixation, which may vary over time in a given location due to variations in temperature or the supply of light. One approach to evaluate the relative contribution of physiological factors vs CO₂ is to produce ϵ_p records from sites of widely contrasting oceanographic setting, where the CO₂ signal may be expected to be common to both locations but the environmental factors such as nutrient availability might not be expected to change in unison. The existing ϵ_p -based CO₂ estimations for the Oligocene are derived from ~ 1 m.y. resolution measurements from two sites on the south American margin of the equatorial and South Atlantic; in the early Miocene an additional North Atlantic record provides data (CenCO2PIP Consortium, 2023). In this study, we produce a new long-term record of ϵ_p over the Oligocene to Miocene time interval at two new, widely separated locations: IODP Site 1406 in the subtropical North Atlantic off the Newfoundland coast, and ODP 1168 in the Southern Ocean off of Tasmania. We also increase the resolution of determinations at the equatorial Atlantic ODP 925.

Our new < 1 m.y. resolution ϵ_p records from these two mid-latitude locations allow us to directly compare ϵ_p with estimates of SST derived from alkenones extracted from the same samples, since unlike very warm tropical locations, the U_{37}^{kl} index still retains sensitivity to temperature in the mid-latitudes during the Oligocene and early Miocene. Additionally, we compare ϵ_p with benthic $\delta^{18}\text{O}$ available from the same sediments, an indicator of high-latitude temperature and Antarctic ice sheet extent and/or volume. These long-term relationships are contrasted with higher resolution analysis during the middle Oligocene at IODP 1406. The dataset allows a robust evaluation of the relationship between ϵ_p and climate dynamics for this time interval. We further discuss the significance of the observed ϵ_p record with the implications for the phytoplankton sensitivity over multimillion year timescales over the Cenozoic.

1.2 An overview of alkenone ϵ_p *p*CO₂ proxy

The carbon isotopic fractionation in phytoplankton during photosynthesis is affected not only by the CO_{2(aq)} but also by physiological factors related to the cellular uptake of carbon. These were initially modelled from the assumption of diffusive carbon acquisition in phytoplankton cells (Rau et al., 1996), where higher ϵ_p could be induced by higher CO_{2(aq)}, lower instantaneous growth rates, or a higher cellular surface area to volume ratio. Both cellular permeability and the carbon isotopic fractionation by the Rubisco enzyme have been assumed to be constant, with Rubisco fractionation typically estimated between 25 and 29 % for alkenone producers (Pagani et al., 2014). Traditional attempts to reconstruct *p*CO₂ from ϵ_p have simplified



80 this original diffusive model by relating ϵ_p and CO_2 with a single factor b defined to include all physiological parameters
affecting the fractionation, and ϵ_f representing the fractionation of the Rubisco enzyme (Jasper and Hayes, 1994).
The b -value has been estimated from modern photic zone and culture samples, for which $\text{CO}_{2(\text{aq})}$ is independently known. For
sedimentary alkenones, previous $p\text{CO}_2$ calculations have either, (1) assumed the modern b -value for that oceanographic setting
remained constant in the past (e.g. Zhang et al., 2013), (2) applied modern relationships between b and phosphate and a
85 simulated paleo-surface ocean phosphate concentration at the site (Pagani et al., 2011), or (3) estimated the difference between
the modern b value at the site and the paleo-setting b value from productivity proxies or proxies for coccolithophore size
(Bolton et al., 2016; Henderiks and Pagani, 2007). Despite the appeal of this approach, a recent re-evaluation of cultures and
field observations suggest the b term is not well predicted by growth rate, light or cell size alone in a diffusive model.
Additional effects occur from carbon concentration mechanisms (CCM) on carbon uptake at lower CO_2 concentrations, which
90 cause a deviation in the CO_2 dependence from the theoretical hyperbolic relationship (Hernández-Almeida et al., 2020; Stoll
et al., 2019). A further challenge to the physical diffusive model is that the Rubisco fractionation in coccolithophores has been
measured in-vitro as 11 ‰ rather than 25‰ (Boller et al., 2011), suggesting that fractionations larger than 11‰ may reflect
the operation of additional enzymatic fractionations (Wilkes et al., 2018). The lower Rubisco fractionation has implications
for the sensitivity of ϵ_p to CO_2 (e.g. as explored in (González-Lanchas et al., 2021)).
95 A meta-analysis of experimental culture data (Stoll et al., 2019) suggests that ϵ_p features a logarithmic dependence on CO_2 ,
rather than the hyperbolic dependence implied by (Rau et al., 1997). This approach does not resolve the mechanisms for the
observed slope of ϵ_p dependence on CO_2 , but over the range of $\text{CO}_{2(\text{aq})}$ from 5 to 30 μM , it provides an empirical relationship
for interpreting the magnitude of $\text{CO}_{2(\text{aq})}$ change implied by a given ϵ_p change. The culture dataset illustrates more broadly how
 ϵ_p is the sum of its dependencies on $\ln(\text{CO}_2)$, $\ln(\text{light})$, and growth rate and cell radius:

100

$$(1) \epsilon_p = 2.66 \ln(\text{CO}_2) + 2.33 \ln(\text{light}) - 6.98 \mu_i - 1.28 \text{radius} + 6.26$$

where $\text{CO}_{2(\text{aq})}$ is in μM , light is in μE , growth rate is day^{-1} and radius is in microns (see Stoll et al. (2019) for confidence
intervals on the regression).

105 From this empirical culture calibration, two challenges remain for the estimation of past CO_2 from ϵ_p measurements derived
from sedimentary alkenones. First, its use would require an estimation of the cell radius, light during the season and depth of
alkenone production, and the growth rate. While cell size can be estimated from coccolith length, determining the absolute
light and growth rate is rarely possible. Since the equation is a linear sum of these influences, these non- CO_2 variables may be
integrated into the intercept (e.g. as in González-Lanchas et al. (2021)), where the intercept (I) would decrease with higher
110 growth rates and larger cell sizes and increase with higher light.

$$(2) \epsilon_p = 2.66 \ln(\text{CO}_2) + I$$

Yet, as with Eq. (1), there remains the challenge of determining which value should be used for the intercept for past conditions,
115 and whether a constant or variable I is more appropriate for a given site since there are limited proxies for algal growth rate.
Recent culture studies document a 0.5 ‰ decrease in ϵ_p per 1°C warming (Torres Romero et al., 2024), a magnitude which is
indistinguishable from the prediction of growth rate effect on ϵ_p and the modeled temperature dependence of coccolithophore
growth rates (Krumhardt et al., 2017). This suggests that growth rate, and I , may vary over time at a given location if
temperature is variable. Therefore, records of SST from alkenone unsaturation or other proxies provide the opportunity to
120 deconvolve the effects of temperature-driven growth rate variations on ϵ_p even when the absolute growth rate is not known.
In this study, given the potential for oceanographic conditions at the studied sites to differ significantly from those in the
modern ocean at these locations, and the concomitant high uncertainties in estimating an appropriate b value for the traditional



approach or I for Eq. (2), we do not calculate the past absolute CO_2 concentration from our ϵ_p measurements. Instead, we account for the potential influence of temperature-driven growth rate changes on our ϵ_p records using alkenone temperature estimates derived from the same samples. Similarly, we evaluate the potential impact of cell size variations on the ϵ_p changes. Then, we employ the sensitivity of ϵ_p to CO_2 in Eq. (2) to estimate possible relative changes in CO_2 in the case where the other nutrient-stimulated growth rate or light influences on ϵ_p were constant during the studied interval at each site evaluating evidences for this assumption.

2 Sites and sediments

We have selected two widely separated paleo locations for this study, from the mid latitude North Atlantic ocean and the high to mid latitudes of the Southern Ocean, from IODP 1406 (40°21.0'N, 51°39.0'W; 3,814 mbsl), ODP 1168 (43° 36.5'S, 144° 24.7'E, and 2463 mbsl) (Fig. 1). A total of 43 and 34 sediment sampling spreading from 30 Ma to 17 Ma at each site were selected. Additionally, higher resolution sampling at IODP 1406 was performed within the 29-30 Ma time window. We also measured an additional six sample set from equatorial Site ODP 925 (4°12.25'N, 43°29.33'W, 3042 mbsl) in order to increase the million-year scale resolution of the previous longest Oligocene record in alkenone carbon fractionation (Zhang et al., 2013). The age model for Sites 1406 and 1168 has been updated using new $^{87}\text{Sr}/^{86}\text{Sr}$ isotope stratigraphy (Stoll et al., 2024) and the age-modelling software Bacon (Blaauw and Christen, 2011). The new age model for IODP Site 1406 is comparable to previously published chronologies (e.g. as in Guitián et al. (2019) and Van Peer et al. (2017)) but clarifies the duration of the upper Miocene hiatus between 33.3 m and 34.7 m core depths (CCSF-A) as extending from 18.5 to 21 Ma. The ODP Site 1168 age model was revised with the Sr isotope stratigraphy in the interval from 562 to 278 mbsf. The Site 1168 chronology is significantly shifted for most of the Oligocene to early Miocene compared with previous biostratigraphically-based age models and shipboard magnetostratigraphy (Pfuhl and McCave, 2003). Strontium isotope stratigraphy identifies a condensed interval from 22.5 to 21.6 Ma, but suggests sustained sedimentation thereafter through 16 Ma. The age model is most uncertain between 27 and 25 Ma where the Sr isotopic curve has a low rate of change. For the two ODP 1168 samples deeper than the Sr isotope measurements, and those from Site ODP 925 we use previous age constraints as published previously by Guitián et al. (2020). The paleolatitude reconstruction for the Oligocene to early Miocene barely changes the position of Atlantic sites, in contrast, ODP 1168 moved from 55°S to 48°S between 30 and 15 Ma (Torsvik et al., 2012; van Hinsbergen et al., 2015). Paleodepth estimates for coastal site ODP 1168 suggest a gradual deepening from the Eocene onwards (Exon et al., 2001).

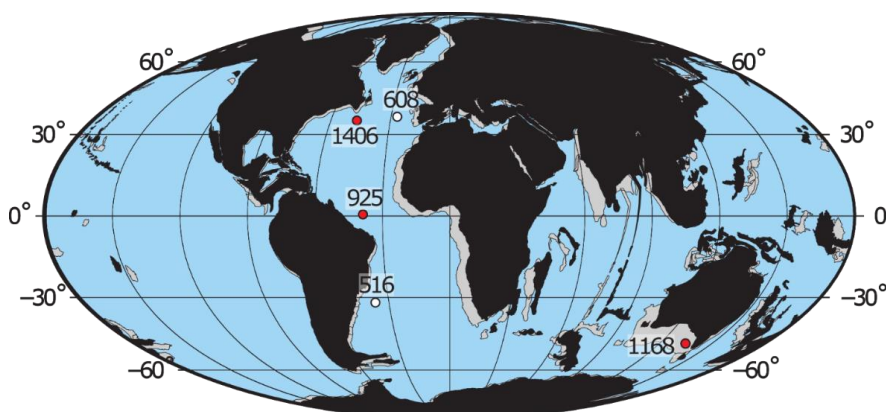


Figure 1. Location of the study sites. Reconstructed map of continental distribution over the 30 Ma (grey) – 17 Ma (black) time interval. Modified after the plate tectonic reconstruction service ODSN.



3 Methods

3.1 Alkenone purification, quantification and $\delta^{13}\text{C}$ analysis

155 Biomarkers from sediments of IODP 1406 and ODP 1168 were extracted from 30g of freeze-dried sediment using an Accelerated Solvent Extractor 350 with $\text{CH}_2\text{Cl}_2/\text{MeOH}$ (9:1 v/v) solvent for four static cycles at 100°C and further silica gel column chromatography protocols for purification of the ketone fraction containing the alkenones (see Guitián et al. (2019) for details).

Alkenone ratios were obtained with a Thermo Scientific Trace 1310 Gas Chromatograph (GC)-FID. Originally, for IODP 160 1406 and 1168 samples the GC-FID was equipped with a non-polar ($60\text{ m} \times 0.25\text{ mm} \times 0.25\text{ }\mu\text{m}$) capillary column (ZB-1ms, Zebron™) at ETH Zurich and at Lamont-Doherty Earth Observatory from Columbia University (Guitián et al., 2019; Guitián and Stoll, 2021). However, ODP Site 1168 samples older than 22.4 Ma featured more complex chromatograms and a high diversity of compounds. To reduce the effects of coelution, samples were additionally analyzed on a 105m column RTX-200ms at ETH Zurich, which improved separation of long chain ketones (Rama-Corredor et al., 2018). The following 165 temperature program was used: 1 min at 50°C , temperature gradient of $40^\circ\text{C}/\text{min}$ to 200°C and $5^\circ\text{C}/\text{min}$ to 300°C , hold for 45min, and increased to 320°C at $10^\circ\text{C}/\text{min}$ and hold for 8min. Carrier gas was Helium at a flow rate of 1.5ml/min. In-house standards and replicates injected at every sequence ensured instrument precision. A subset of IODP Site 1406 and samples younger than 22.4 Ma from Site 1168 were re-measured with the RTX-200 to ensure replicability (Table S1). Method used for each organic analysis is described in the supplementary material dataset.

170 **Sea surface temperature** was calculated from U_{37}^{kt} ratio using the Bayspline calibration (Tierney and Tingley, 2018) for all samples in IODP 1406 and for the young set of samples in ODP 1168. Because for those, we find U_{37}^{kt} ratios within the analytical uncertainty using both columns, we report the original ZB-1 results for all Site 1406 samples and Site 1168 samples younger than 22.4 Ma / 408.22 m depth. The RTX-200 column provided substantially improved resolution of C38 peaks, allowing quantification of $\text{C}_{38:2}$ and $\text{C}_{38:3}$ ME peaks, but for samples between the ages of 23.1 and 29.1 Ma in ODP 1168 it did 175 not perform well enough for the C37 peaks. Therefore, for this set we provide temperatures estimated from the U_{38ME}^{kt} ratio applying the Novak et al. (2022) core top calibration. For the ODP 925 equatorial site samples, the $\text{C}_{37:3}$ methyl ketone is under the detection limit, therefore we further purified and analyzed the extracted organics as in Guitián et al. (2019) to get the temperatures from the TEX86 ratio using the BAYSPAR calibration by (Tierney and Tingley, 2015).

Compound-specific $\delta^{13}\text{C}$ measurements were performed on a Thermo Scientific Trace 1310 Gas Chromatograph coupled to 180 a Thermo Scientific GC Isolink II, a Conflo IV, and a Delta V Plus Mass Spectrometer at ETH Zurich. Oxygen was flushed through the combustion reactor for one hour at the beginning of each sequence and seed oxidized for one minute before each injection. Alkenones from ODP Site 1168 and IODP 1406 were analyzed on a GC equipped with a non-polar capillary column ($60\text{ m} \times 0.25\text{ mm} \times 0.25\text{ }\mu\text{m}$) (ZB-1ms, Zebron™) and 5-m guard column. Helium was used as carrier gas flow with 2-ml/min. GC oven was set at 90°C ramped to 250 at $25^\circ\text{C}/\text{min}$, to 313°C at $1^\circ\text{C}/\text{min}$ and finally to 320°C at $10^\circ\text{C}/\text{min}$. The GC oven 185 was then maintained isothermally for 20 min. A subset of IODP 1406 samples were measured additionally at the Lamont-Doherty Earth Observatory on equivalent instrumentation but with some modifications for improved sensitivity (Baczynski et al., 2018) and following similar GC procedures, with similar results.

From ODP Site 1168, a subset of samples older than 24.5 Ma featuring more complex chromatograms were rerun on a GC-irMS equipped with a RTX-200 ms column. GC oven was set at 50°C ramped to 275°C at $40^\circ\text{C}/\text{min}$, to 295°C at 0.5°C , hold 190 for 22 min, and finally ramped to 320°C at $10^\circ\text{C}/\text{min}$ and hold for 5 min. Flow rate was 1.5ml/min. Comparison of a subset of samples from Site 1406 and ODP 1168 younger than 22.4 ma showed that $\delta^{13}\text{C}$ C37:2 were similar on both ZB-1 and RTX-200 columns. We consequently report here $\delta^{13}\text{C}$ C37:2 from the ZB-1 runs, with the exception of the samples from Site 1168 older than 22.4 Ma. All values are reported here in parts per mil (‰) relative to VPDB (Vienna Pee Dee Belemnite). Sample



replicates, in-house alkenone standard (provided by G. O'Neil, Western Washington University, and C. M. Reddy, Woods
195 Hole Oceanographic Institution), and known isotopic mixtures A5 and B4 (supplied by A. Schimmelmann, Univ. of Indiana)
were simultaneously measured to determine the analytical accuracy of the measurement and an uncertainty of 0.5 ‰.

3.2 Estimation of aqueous carbon dioxide $\delta^{13}\text{C}$

Isotopic composition of $\text{CO}_{2[\text{aq}]}$ is estimated from the temperature dependent fractionation between DIC and aqueous CO_2
during alkenone production of Rau et al. (1996) based on Mook et al. (1974) and Freeman and Hayes (1992):

$$200 \quad (3) \quad \delta^{13}\text{C}_{[\text{CO}_2]_{\text{aq}}} = \delta^{13}\text{C}_{\text{DIC}} + 23.644 - \left(\frac{9701.5}{T}\right)$$

The $\delta^{13}\text{C}$ DIC may be estimated from the $\delta^{13}\text{C}$ of calcium carbonate of benthic foraminifera with the assumption of a constant
and known offset between the $\delta^{13}\text{C}$ DIC of the deep and surface ocean, or from bulk sediment calcium carbonate that is mostly
derived from coccolithophores and planktonic foraminifera. Site 1406 and 925 features sufficient well preserved benthic
foraminifera, mainly epifaunal *Cibicidoides* spp. larger than 200 μm , $\delta^{13}\text{C}$ of surface ocean DIC can be calculated here applying
205 a constant offset of 2 ‰ of measurements from the same samples following previous Miocene and Oligocene studies (Gutián
et al., 2019; Pagani et al., 2011; Zhang et al., 2013). However, at ODP Site 1168 benthic foraminifera were scarce for picking
for isotopes in many intervals and the progressive evolution of water depth at the site may change the $\delta^{13}\text{C}$ offset between the
benthic environment and the surface ocean over time. Consequently, to follow the same approach for all studied records we
calculate the $\delta^{13}\text{C}$ DIC from the $\delta^{13}\text{C}$ of the bulk carbonate, which is dominated by *Reticulofenestra* coccoliths (Gutián et al.,
210 2020). Because there is no divergence of vital effects between small and large coccoliths in the late Oligocene to early Miocene
(Bolton and Stoll, 2013), we propose that the offset between coccolith $\delta^{13}\text{C}$ and DIC is likely to remain constant. We subtract
0.5 ‰ from the $\delta^{13}\text{C}_{\text{bulk}}$ to calculate $\delta^{13}\text{C}_{\text{DIC}}$, based on average alkenone-producing coccoliths cultured at DIC <4 mM compiled
in Stoll et al. (2019). Support for estimating photosynthetic fractionation from coccolith $\delta^{13}\text{C}$ is provided by recent culture
studies of *G. oceanica* (Torres Romero et al., 2024).

215 Stable isotopes of carbonates were measured as described in in Gutián et al. (2019) with the guidelines from Breitenbach and
Bernasconi (2011) for small carbonate samples on a GAS BENCH II Delta V Plus irMS from Thermo Scientific with
international (NBS-19 & 18) and in-house carbonate as standards achieving a precision of 0.07 ‰.

3.3 Calculation of ε_p 37.2

Carbon isotopic fractionation (ε_p), describes the fractionation occurring during photosynthesis when carbon is fixed into algal
220 cellular biomass ($\delta^{13}\text{C}_{\text{org}}$) from the ambient aqueous CO_2 ($\delta^{13}\text{C}_{\text{CO}_2\text{aq}}$) (Freeman and Hayes, 1992):

$$(4) \quad \varepsilon_p = \left(\frac{(\delta^{13}\text{C}_{[\text{CO}_2]_{\text{aq}}} + 1000)}{(\delta^{13}\text{C}_{\text{org}} + 1000)} - 1\right) * 1000$$

Organic $\delta^{13}\text{C}$ is obtained from the $\delta^{13}\text{C}$ analysis of haptophyte specific alkenone di-unsaturated $\text{C}_{37.2}$. Culture experiments
showed that the lipid organic matter is depleted in ^{13}C relative to the whole cell isotopic composition by 4.2 ‰, a correction
that needs to be applied (Popp et al., 1998; Wilkes et al., 2018):

$$225 \quad (5) \quad \delta^{13}\text{C}_{\text{org}} = [(\delta^{13}\text{C}_{37.2} + 1000) * ((4.2/1000) + 1) - 1000]$$

Uncertainties were propagated by a full Monte Carlo ($n = 10000$) simulation following (Tanner et al., 2020).

To compare our new records with previous data spanning the same time interval, we discuss published ε_p datasets recently
compiled by the paleo CO_2 community (Cen CO_2 PIP Consortium, 2023), from DSDP 516 in the South Atlantic (Pagani et al.,
2000; Pagani et al., 2011; Pagani et al., 2005), DSDP 608 in the North Atlantic (Super et al., 2018), and the equatorial site
230 from ODP 925 (Zhang et al., 2013). For these, we ensure that ε_p for the published records is calculated from biomarker-based



paleothermometers. The most recent publications from DSDP 608 and 925 used GDGT-derived estimations from TEX-86. To better compare our results with DSDP 516, where originally temperatures were derived from $\delta^{18}\text{O}$ of planktic foraminifera for the Miocene section and GDGTs for part of the Oligocene, we have updated the ε_p calculations using a running averaging of the recent higher resolution GDGT temperature reconstructions from Auderset et al. (2022) at the same site.

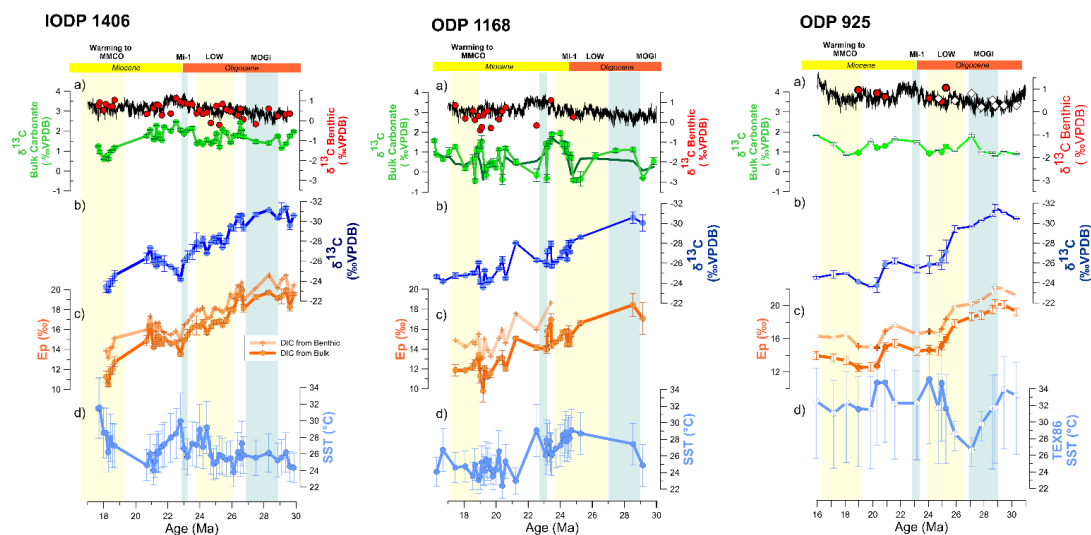
235 For our data of paired ε_p and alkenone SST, we calculate the shift in ε_p which is expected from temperature-stimulated growth rates. We adjusted each samples ε_p absolute value by using the relationship of -0.48‰ per 1°C SST difference relative to the record average (Torres Romero et al., 2024). We complete a similar exercise for cell radius, calculating the deviation in ε_p relative to the median cell size, for each point using the culture dependence of ε_p on cell radius (Stoll et al., 2019). Biogenic silica (bioSi) was determined on 20 samples from ODP 1168 following methods described previously in Guitián et al. (2020).

240 4 Results and Discussion

4.1 Trends in ε_p in the Oligocene to early Miocene

4.1.1 New ε_p records from sites 1406 and 1168

In both long-term records from Site 1406 and Site 1168, $\delta^{13}\text{C}$ of $\text{C}_{37.2}$ alkenones range from very low values near -30‰ in the early Oligocene (28-30 Ma) increasing to -24‰ by 18-20 Ma (Fig. 2). The new calculated ε_p decrease from the Oligocene to
245 the early Miocene, defined most precisely at the highest resolution North Atlantic Site 1406, features abrupt 3‰ declines from 26.5 to 25.4 Ma and 24 to 22.8 Ma. Newly obtained ODP 925 ε_p determinations within the interval 25 Ma to 19 Ma are in agreement with previous determinations at this site (Zhang et al., 2013) resolving steps at 26 Ma and 21 Ma. The trends in ε_p calculated from benthic $\delta^{13}\text{C}$ are similar to those calculated from the coccolith-dominated bulk $\delta^{13}\text{C}$. In the high resolution section from 28.8 to 29.6 Ma in Site 1406 there is no long-term trend, but orbital scale ε_p variations exceed 1.5‰ in amplitude
250 (Fig. 3, Fig. S1). Several-100 ky orbital scale variations of 0.75‰ benthic $\delta^{18}\text{O}$ and bulk $\delta^{18}\text{O}$ are sampled, as expected for this time window of high 100 ky power in benthic $\delta^{18}\text{O}$ in other sites (Liebrand et al., 2017).



255 **Figure 2: Analytical results of this study. a)** Carbonate stable isotopes for benthic foraminifera (red symbols), data from this work for each site; black line shows results from Westerhold et al., (2020) and bulk sediment carbonate (green color). **b)** Alkenone $\text{C}_{37.2}$ $\delta^{13}\text{C}$. **c)** Calculated alkenone carbon fractionation, solid line DIC $\delta^{13}\text{C}$ is derived from bulk carbonate, transparent line from picked benthic foraminifera at the same samples. **d)** Temperature estimates. IODP 1406, including SST and benthic $\delta^{18}\text{O}$ dataset from Guitián et al., (2019); ODP 1168, dark green $\delta^{13}\text{C}$ bulk carbonate shows the 4-point moving average used to calculate ε_p at the site; ODP 925, filled circles are new measurements for this study, white symbols are published data (Zhang et al., 2013), being ε_p



260 recalculated following method described in text. Note SST is derived from GDGT at this site. SST errors bars: 1406- 1σ , 1168- $U_{37}^{K'}$ -
 1σ , 1168- $U_{38ME}^{K'}$ - 2σ , 925-TEX₈₆- 2σ .

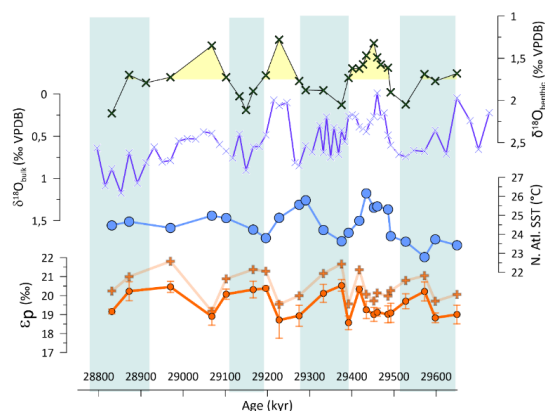


Figure 3. High resolution sampling from IODP 1406, showing $\delta^{18}\text{O}$ of bulk carbonate and benthic foraminifera, alkenone SST estimates, and ϵ_p calculated from bulk carbonate (circles) and benthic foraminifera assuming a constant offset (crosses).

4.1.2 Comparison of 1168 and 1406 ϵ_p records with published Atlantic records

265 The overall decline in ϵ_p through the time interval of our records, is broadly comparable to the trend in published ϵ_p datasets recently compiled by the paleo CO_2 community (CenCO2PIP Consortium, 2023), which exhibits a long term decrease in the late Oligocene through the transition to the Miocene and an overall low and stable early Miocene (Fig. 4). However, several factors complicate a detailed comparison of our new and the previously published records.

270 Rapid ϵ_p shift comparison might be hindered by site chronology uncertainties. Although all records are presented here on the GTS 2012 (Gradstein et al., 2012), ODP 1168 and IODP 1406 age models rely on Sr isotope stratigraphy (Stoll et al., 2024), whereas ODP 925, DSDP 516 and ODP 608 are based exclusively on biostratigraphic and magnetostratigraphic reversals datums (Curry et al., 1995). As seen in sites 1168 and 1406, Sr isotopic stratigraphy can adjust age determinations by 0.5 to 1 Myr. or even up to 2 Myr. at few cases.

275 Additionally, differences in the absolute value of ϵ_p among records may also reflect contrasting approaches to the reconstruction of DIC $\delta^{13}\text{C}$ in the different studies. At DSDP 608, the DIC $\delta^{13}\text{C}$ was reconstructed from surface-dwelling foraminifera *G. quadrilobatus* (Pagani et al., 1999), while at DSDP 516 the Miocene section was estimated from planktic foraminifera and most of the Oligocene samples DIC $\delta^{13}\text{C}$ was determined from fine fraction (Pagani et al., 2000; Pagani et al., 2005). Published ODP 925 ϵ_p has been recalculated here with DIC $\delta^{13}\text{C}$ derived from bulk carbonates of nearby samples, to resolve the previous divergent estimates from planktic and benthic foraminifera (Zhang et al., 2013).

280 The longest record from **DSDP Site 516** exhibits a general ϵ_p decline from the Oligocene to early Miocene. However, due to lower resolution at this site, we cannot evaluate if there is an abrupt 3 ‰ decline from 26 to 24.5 Ma as seen in sites 1406 and 925. A steep ϵ_p decline between at 21 and 20 Ma in Site 516 may be within age uncertainty of the decrease observed at ODP 1168 and ODP 925; additional Sr isotope stratigraphy at Site 516 in this time interval could help test the synchronicity. The late Oligocene at DSDP 516 features a 5‰ peak in ϵ_p between 24.5 and 24.9 Ma, which is not reflected at 1406, or 1168 sites.

285 The early Miocene record at **DSDP Site 608** shows a more variable ϵ_p with a much steeper decline through the early Miocene and higher amplitude variation compared to other sites. The characteristic minimum in ϵ_p from 18 to 17 Ma is potentially within the age model uncertainty of the minimum in ϵ_p at 19 Ma in 1168 and the minimum identified at Site 1406 at 18.5 Ma. Updated stratigraphy could contrast more robustly the timing of these events. If there is high amplitude short term variability



in ϵ_p in the early Miocene as in the Oligocene time interval (Fig. 2), there is also the potential for low resolution sampling to
 290 undersample high frequency temporal variability and generate aliasing artefacts.

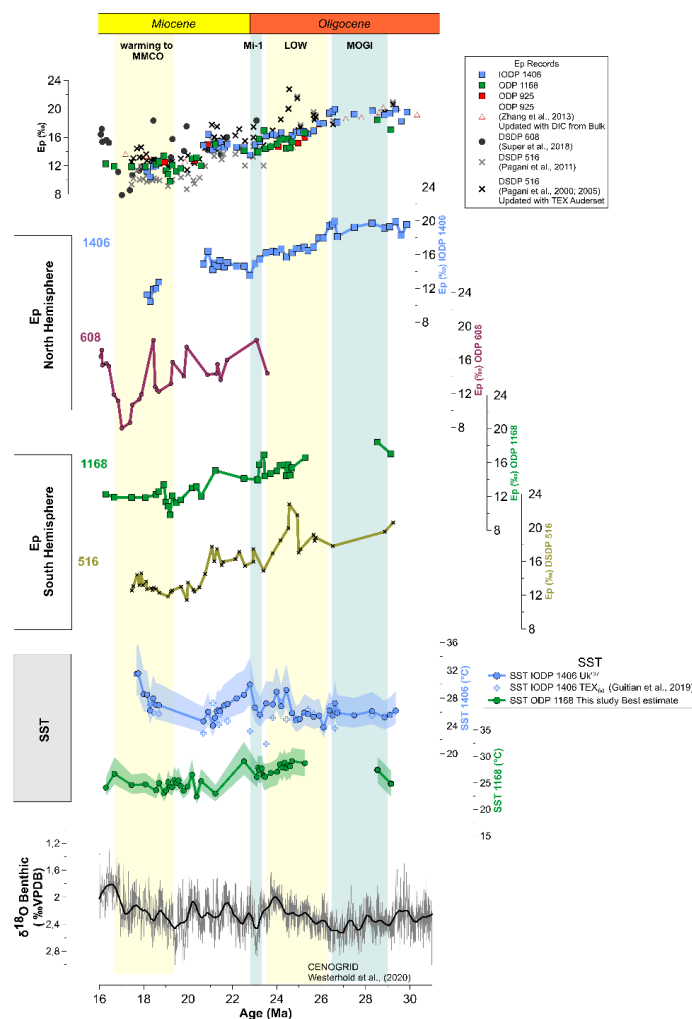


Figure 4: Oligocene to Miocene global long term ϵ_p trends. Comparison of the new obtained ϵ_p records with previously published alkenone measurements. All ϵ_p estimates have been recalculated following the methodology described in text with data source described on Table S2.

295 **4.2 CO₂ vs size and nutrient effects on ϵ_p**

In addition to CO₂, ϵ_p may be influenced by changes in cell surface area to volume ratio and cellular growth rate regulated by light and nutrients. There is no long-term trend in mean coccolith size in these records (Gutián et al., 2020) and estimating the impact of it on the ϵ_p records shows a negligible effect on long-term trends (Fig. 5). At discrete time intervals of IODP Site 1406, the size effect reduces most values older than 27 Ma and produce a steeper decrease on ϵ_p towards the Oligocene Miocene
 300 transition.

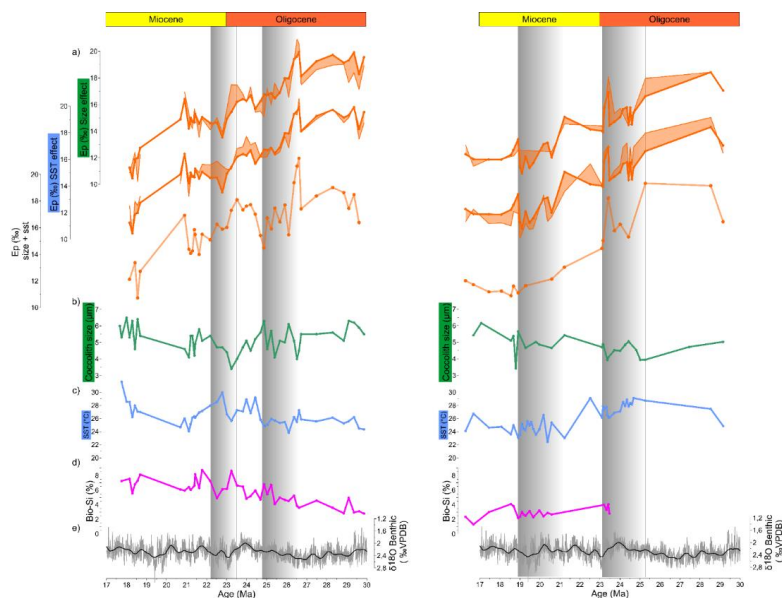
For the statistical model of Eq. (1), it is complex to identify proxy records for any possible effect of nutrient-stimulation of growth rate or changes in the mean light conditions at the depth of growth. In modern spatial gradients in the ocean, these factors are often coupled, so that settings characterized by deep mixing and high nutrient supply rates to stimulate growth, are also characterized by lower mean light levels due to the deeper mixing, both factors lowering ϵ_p .



305 As one possible nutrient indicator, a higher concentration of biogenic silica (bioSi) in sediments may reflect a higher rate of
bioSi delivery to the seafloor due to higher export production produced by siliceous organisms (mainly diatoms) in the ocean
(Ragueneau et al., 2000). In the modern ocean, regions with abundant dissolved Si in the photic zone are regions also
310 in surface waters at the site (Fig. 5). If the increase in dissolved silica observed at the North Atlantic is correlated to an increase
in dissolved P or N, it could contribute to increase in growth rate, and therefore likely increase in biomass and chlorophyll,
which would reduce light in the water column both being part of the observed long term decrease of ϵ_p . However, the actual
correlation between bioSi and ϵ_p is not that strong (Fig. S2), suggesting that while increased nutrient concentrations could
contribute to the long-term evolution of ϵ_p , the specific steps of ϵ_p decline are less likely to be driven by increased nutrients
315 and growth rate.

The drivers for increasing bioSi burial rates at Site 1406 are not clear, although they could reflect a global increase in nutrient
delivery. Important changes in the rate of continental weathering within the Oligocene- early Miocene are often interpreted
from the evolution of radiogenic isotopes of Sr, Li and Os (Misra and Froelich, 2012) including the steep rise in $^{87}\text{Sr}/^{86}\text{Sr}$,
although the precise origin of the late Eocene and Miocene increase in $^{87}\text{Sr}/^{86}\text{Sr}$ remains under discussion (Rugenstein et al.,
320 2019). On a global scale, the nutrient delivery may be conditioned by the riverine supply of P from continental erosion and
weathering of P containing minerals. On the time scales examined in our records, much longer than the residence time of P,
the net effect on nutrient concentrations depends on the balance of the supply and the nutrient removal in sediments.

While a significant increase in erosion and weathering and nutrient inventory is one mechanism to contribute to the long term
decline in ϵ_p via enhanced algal growth rates, an increase in erosion and weathering can itself contribute to a CO_2 drawdown
325 by CO_2 consumption through silicate weathering and enhanced burial of organic carbon in delta regions (Raymo and
Ruddiman, 1992). If the biogenic Si increase at 1406 were representative of a global trend, an increase in nutrient supply may
have contributed to ϵ_p decline through both CO_2 decline and increased nutrient stimulation of phytoplankton growth. A global
decline in ϵ_p solely from increased weathering and nutrient concentrations without a CO_2 decline would require that in the
Oligocene, the nutrient release from silicate weathering was less coupled to carbon burial than in the late Neogene. If the
330 periodically glaciated margin of Antarctica is a major locus for increased erosion and weathering in the Oligocene (Reilly et
al., 2002), release of nutrients and radiogenic isotopes may have occurred in the continental margins, but with much less
organic carbon burial than the modern Himalaya system due to limited terrestrial biomass on Antarctica and temperature and
sea-ice limited oceanic biomass production in the marine regions.



335 **Figure 5:** Timeseries of ϵ_p at IODP 1406 and ODP 1168 including a) the measured ϵ_p record (solid line) and the estimated ϵ_p resulted
once size and temperature effect is applied following Torres et al., (2024), and Stoll et al., (2019) (transparent shadows). b) Coccolith
size record from Guitian et al., (2020); c) SST estimates d) Biogenic silica measurements (Guitian et al., (2020) and this study); e)
reference CENOGRID benthic $\delta^{18}\text{O}$ curve (Westerhold et al., 2020)

On the other hand, the long term trend of increased bioSi is not observed in the Southern ocean Site 1168 (Fig. 5). The available
340 Miocene bioSi at ODP 1168 is stable with no change across the steep ϵ_p drop from the latest Oligocene to early Miocene. The
increasing distance of Site 1168 from the coastline with basin subsidence may have decreased the availability of Si from the
early Oligocene through the early Miocene, imparting a local effect superimposed on any potential global trend. However,
likely not only Si but also other nutrients would decrease with increasing distance from the coast. If the long term trend in ϵ_p
at both 1406 and 1168 sites were conditioned by increased nutrient availability, faster growth rates, and lower light levels it
345 would require bioSi accumulation rates at Site 1168 to be decoupled from the overall changes in nutrient availability, which
we consider less likely. Consequently, we propose that the similarity in trend and magnitude of the long term ϵ_p decline in both
sites (and in tropical Site 925), is more consistent with a global forcing of ϵ_p , which may be most plausibly driven by a
significant decrease in atmospheric CO_2 and CO_2aq .

4.3 Relationship between ϵ_p and SST and benthic $\delta^{18}\text{O}$

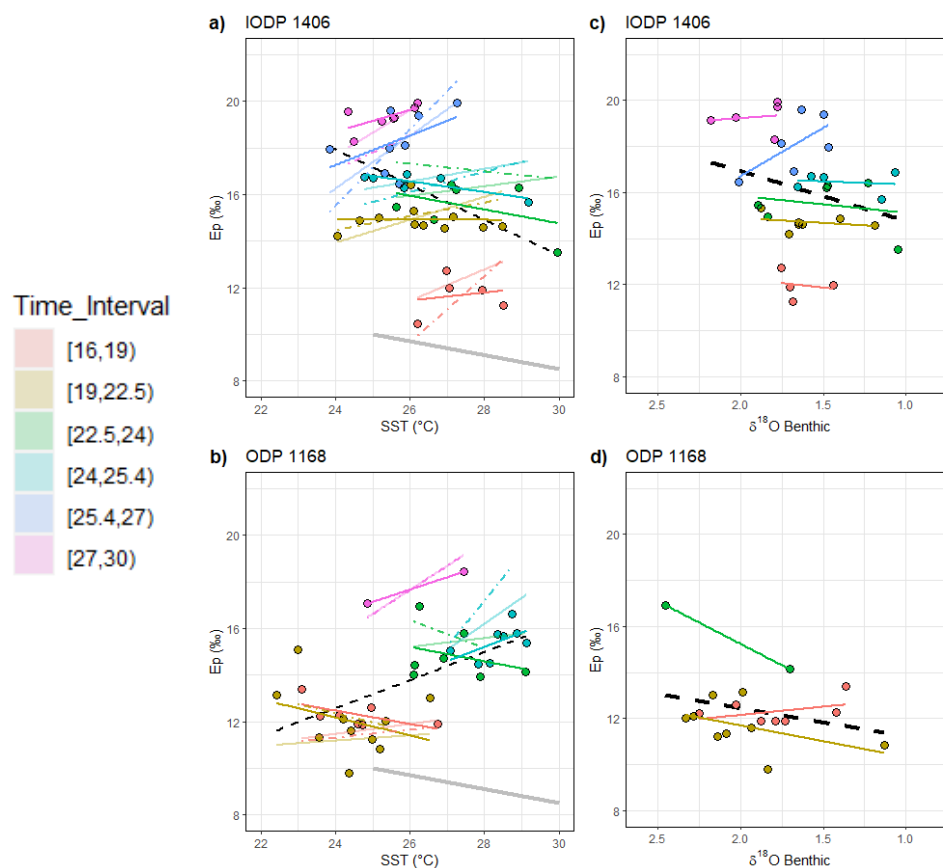
350 The new ϵ_p data from Site 1406 and Site 1168 provide the first records of ϵ_p from the early Oligocene to early Miocene with
alkenone unsaturation indices as independent estimations of SST for the precise time intervals of ϵ_p determination. Since they
are biomarkers derived from the same organism, alkenone-derived SST estimates correspond to the same season and growth
depth as the alkenone ϵ_p determinations. There are two processes which may influence the relationship between temperature
and ϵ_p . First, higher temperatures lead to higher phytoplankton carbon fixation rates, decreasing ϵ_p . Secondly, higher CO_2
355 would increase ϵ_p and through radiative forcing lead to warmer global average temperature and SSTs. The expected relationship
between ϵ_p and SST from either process could be obscured by a superposition of temperature effects on growth rate and a
climatic correlation of ϵ_p with mean air temperature.

4.3.1 Million year scale relationships

Across the overall time interval, Site 1406 ϵ_p is weakly inversely correlated with SST, whereas Site 1168 ϵ_p is weakly positively
360 correlated with SST (Fig. 6; Fig. S3, Table S3). Our estimation of the growth rate effect due to warmer temperatures shows



that it has a very limited impact on the long term ϵ_p trend, amplifying slightly the long-term excursion in ODP 1168 and imparting a minor increase in ϵ_p in the late Oligocene 25.5 to 24 Ma in IODP 1406 but otherwise not affecting the sign of the overall trend (Fig. 5, 6, Fig. S3). At our studied sites across the 30 to 17 Ma time interval, the long term average warming of 2-3°C is insufficient to account for the 7 ‰ decline in ϵ_p due to a temperature-driven growth rate effect.



365

Figure 6. Relationship between calculated ϵ_p and SST and benthic $\delta^{18}\text{O}$ for the same samples from IODP 1406 and ODP 1168. Dashed dark line in the plot background shows the regression of the overall dataset. Grey line in a) b) shows empirical temperature-growth rate effect in temperature described in the text (Torres et al., 2024) as the ϵ_p change with growth rate if CO_2 were constant. Colored lines shows the regression at specific time intervals for the measured ϵ_p (solid), ϵ_p with the temperature effect removed (transparent), and ϵ_p with both the temperature and size effect removed (dashed). See Fig. S3 for overall dataset relationships.

370

Yet aside from the overall inverse correlation at IODP 1406, during certain time intervals the correlation is positive. Before 25.4 Ma, there is a general positive correlation between ϵ_p and alkenone SST (Fig. 6, Table S3); for the intervals 27 to 30 and 25.4 to 27 Ma in Site 1406 with a slope of 0.7 (n=6, n=10). This is also true for the 25.4 to 24 Ma interval in 1168 with 0.6 slope (n=6). This slope is significantly greater when the influence of size and temperature-growth rate effects on ϵ_p are removed. In other time intervals, there is a negligible slope or negative slope with measured ϵ_p , for example -0.3 (24 to 22.5 Ma in both sites, n=7, n=4) or during the drop after 19 Ma at IODP1406 appear to occur at times of warming temperature (slope= 0.2, n=5) that slightly improves when the ϵ_p is adjusted to size and temperature.

375

Over the studied time interval, this relationship similarly shows insignificant correlation for the previously published ϵ_p records with updated age models and ϵ_p calculations (Fig. S4), although temperatures estimates are derived from GDGT which might not reflect the same depth and/or season of coccolithophore growth. Negative covariance is observed at DSDP 608 from

380

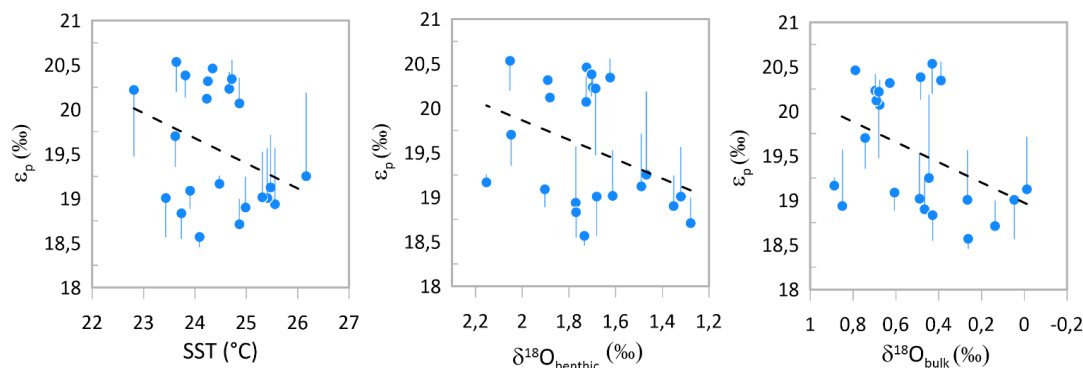


19 to 16 ma, at DSDP 516 before 21 Ma and for the few samples from 27 to 24 ma at ODP 925. Some of these intervals feature significant temperature changes of 4 to 5°C, and therefore the temperature-growth rate effect on ϵ_p may be significant, and the negative slopes observed in some intervals are consistent with this being the dominant effect (gray line in Fig. 6a and 6b). At 385 1406, during the older intervals of positive correlation of SST and ϵ_p , potentially the growth rate stimulation due to higher SST was balanced by a decrease of nutrient availability during warmer temperatures as suggested by the bioSi evolution (Fig. S2), whereas during younger time intervals, temperature exerted a dominant effect on growth rate.

Benthic $\delta^{18}\text{O}$ was measured in multiple time intervals in Site 1406. Benthic $\delta^{18}\text{O}$ has been proposed to reflect global surface temperature (Evans et al., 2024; Hansen et al., 2013) and as such may be less sensitive than SST to regional reorganizations of heat transport. Alternatively, benthic $\delta^{18}\text{O}$ has been proposed to be highly sensitive to the areal extent of the Antarctic ice sheet due to its cooling effect on surface ocean temperatures in regions of deepwater formation (Bradshaw et al., 2021; Lisiecki and Raymo, 2005; Shackleton, 1987). If the global surface temperature change translated to changes in surface ocean temperatures at Site 1406 and Site 1168, we would expect the temperature-growth rate effect to generate a direct correlation between benthic $\delta^{18}\text{O}$ and ϵ_p . If the radiative forcing effect on global temperature change were dominant, we would expect an 390 inverse correlation between ϵ_p and benthic $\delta^{18}\text{O}$. As for SST, only the time intervals older than 25.4 Ma exhibit the inverse correlation expected from radiative forcing, whereas other intervals suggest neutral slope which may reflect the superposition of growth rate and CO_2 -radiative effects on ϵ_p . 395

4.3.2 Relationships between ϵ_p , temperature and benthic $\delta^{18}\text{O}$ at orbital timescales

In the high resolution sampling between 29.0 and 29.6 Ma, despite a significant 1 ‰ range in $\delta^{18}\text{O}$ benthic and $\delta^{18}\text{O}$ bulk, we 400 likewise observe no inverse relationship between ϵ_p and $\delta^{18}\text{O}$ benthic, or between ϵ_p and $\delta^{18}\text{O}$ bulk (Fig. 7). We also observe no significant correlation between ϵ_p and alkenone SST. Because the magnitude of SST variation is small over this time interval, the impact of temperature-stimulated carbon fixation rates is not a significant impact on the relationship between ϵ_p and any of these variables – a temperature-corrected ϵ_p record for the 29 to 29.6 Ma interval would still not exhibit an inverse relationship between ϵ_p and $\delta^{18}\text{O}$ benthic as observed in the late Pleistocene glacial cycles (Hernández-Almeida et al., 2023). 405 If ϵ_p variations are dominantly responding to CO_2 , our results suggest that low CO_2 is not contributing to greater ice volume and/or colder ocean temperatures on 100 ky cycles and that the relationship between Antarctic ice growth and CO_2 may be more complex at this time.



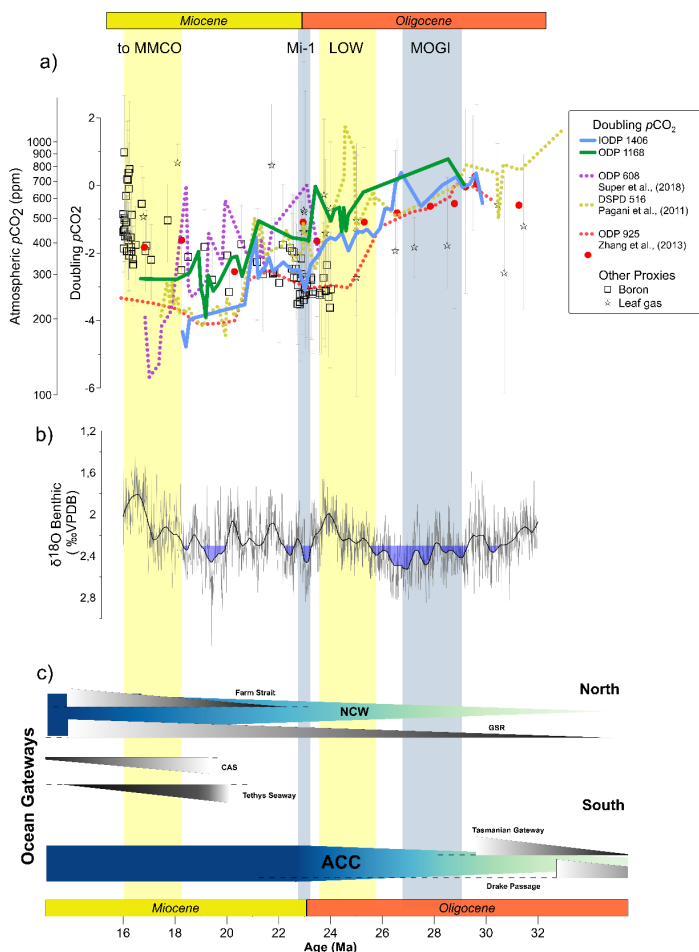
410 **Figure 7. Relationship between calculated ϵ_p and temperature ($r^2=-0.34$), $\delta^{18}\text{O}$ from benthic foraminifera ($r^2=0.42$), and $\delta^{18}\text{O}$ from bulk carbonates ($r^2=0.37$) for the high resolution interval samples from IODP 1406. Vertical error bars shows the temperature effect on ϵ_p following findings from cultures (Torres et al., 2024). Dashed line shows the linear regression for all plotted samples.**



4.4 A Climate and CO₂ paradox from the Oligocene to early Miocene

The long term trends between 30 and 16 Ma based on new ϵ_p data at two sites and recalculation of previous ϵ_p studies with uniform methods cannot be attributed to a temperature effect on growth rate and ϵ_p , nor to changes in the cell size of the alkenone producing community. Both effects are small in magnitude according to the sensitivities observed in cultures and do not alter the long-term trend (Fig. 5). Therefore, the long-term ϵ_p decline must have a significant global driver, with the most obvious being a decline in $p\text{CO}_2$.

Although the calculation of absolute CO₂ concentrations from ϵ_p in the Oligocene and early Miocene remains challenging, the logarithmic dependence of ϵ_p on CO_{2(aq)}} observed in cultures allows us to estimate the relative changes in CO₂ if the sensitivity of ϵ_p to CO₂ in the Oligocene were similar to modern cultured species. If we incorporate a temperature correction on growth rate (Krumhardt et al., 2017) equivalent to the magnitude from cultures (Torres Romero et al., 2024) and apply the 50th percentile estimate of the modern culture ϵ_p dependence on $\ln[\text{CO}_{2(aq)}]$ of 2.66, it implies major changes in CO₂ concentrations, with potentially 4 halvings of CO₂ concentration from 29 to 16 Ma (Fig. 8). Modern General Circulation Models (GCM) estimate climate sensitivity at 3 to 5°C per doubling or halving of CO₂, which if representative for the Oligocene to early Miocene, would imply 12 to 20°C of cooling of earth's mean surface temperature. Although ocean is 70% of the globe and temperature changes are 1.3- to 1.8-fold less than land temperature (Sutton et al., 2007), such a large temperature change of at least 10.4°C would be expected to be reflected in paleoceanographic proxies. Application of the lower confidence interval of modern culture ϵ_p dependence on $\log(\text{CO}_{2(aq)})$ of 3.5, would imply 3 halvings of CO₂, with a correspondingly lower magnitude of change in temperature.



430

Figure 8: Implications of CO₂ as main climate driver. a) Shows pCO₂ doubling compared to previous estimates compiled in CenCO2PIP Consortium, (2023) (Erdei et al., 2012; Greenop et al., 2019; Liang et al., 2022a; Liang et al., 2022b; Londoño et al., 2018; Morawek et al., 2019; Reichgelt et al., 2020; Roth-Nebelsick et al., 2014; Sosdian et al., 2018; Steinhorsdottir et al., 2021; Sun et al., 2017; Tesfamichael et al., 2017; Zhang et al., 2013). Only long term records from alkenone derived CO₂ are recalculated. 435 b) Benthic δ¹⁸O global compilation (Westerhold et al., 2020). c) Schematic representation of main paleoceanographic and paleogeographic changes over the studied time interval for the Northern and Southern Hemisphere. ACC: Antarctic Circumpolar Current. NCW: Northern Component Water.

The late Oligocene climate and CO₂ paradox has been discussed based on previously published lower resolution ε_p record from Site 925 (O'Brien et al., 2020). Our new results from two additional sites confirm the steep CO₂ decline through the late 440 Oligocene warming and underscore the paradox. On a global scale, biomarker SST estimates do not show evidence for systematic cooling during the CO₂ decline (Gutián et al., 2019; Liu et al., 2018; O'Brien et al., 2020). If the interpretation of ε_p as a CO₂ decline is correct, it suggests a very different set of feedbacks and climate sensitivity during this time, or widespread regional heat transport effects on regional temperatures or significant misinterpretation of measured biomarker temperature signals. During this time the inferred CO₂ decline also coincides with sequence stratigraphic evidence for ice margin retreat in 445 Antarctica (Levy et al., 2019; Salabarnada et al., 2018), and sea level transgressions inferred from estimates of deep sea δ¹⁸O_{sw} and Mg/Ca records (Miller et al., 2020), suggesting a substantially different relationship between ice expansion and CO₂ than characterized the late Neogene.



450 For the late Oligocene to early Miocene, the Southern Ocean Site 1168 is the only surface ocean temperature record which exhibits a long-term decline in SST coincident with the record of a large magnitude $p\text{CO}_2$ decline and decline in radiative forcing from the greenhouse effect. This long term cooling is despite the equatorward drift of the site over this time interval (Guitián and Stoll, 2021). Potentially, the ODP Site 1168 temperature trend reflects global temperature during the CO_2 decline, and whereas the long term alkenone temperature record at Newfoundland Ridge Site 1406 and Site 1404 (Liu et al. 2018) is
455 affected by variations in the heat transport from the Gulf Stream that overwhelms the signal of radiative greenhouse forcing. While there is no evidence of a concomitant long term cooling in the benthic $\delta^{18}\text{O}$ series (e.g. Westerhold et al. (2020)), the ε_p minimum at 19 Ma coincides with a local maximum in benthic $\delta^{18}\text{O}$.

A decoupling was at one time proposed for the late Miocene based on apparent negligible $p\text{CO}_2$ change and substantial cooling of SST (LaRiviere et al., 2012). Revisions of the alkenone carbon fractionation to CO_2 calibration approaches for low $p\text{CO}_2$
460 periods have refined the record from the last 15 Ma, revealing clear $p\text{CO}_2$ -SST covariation (Rae et al., 2021; Stoll et al., 2019). However, the Oligocene paradox is not easily resolvable from updated calibration of the ε_p - CO_2 relationship because the late Oligocene divergence arises from an inverse correlation between ε_p and SST reconstructions. Therefore, continued re-evaluation of SST records and interrogation of biogeochemical cycles potentially affecting the growth and physiology of alkenone producers, are needed to reconcile climate sensitivity to CO_2 in the Oligocene to early Miocene.

465 **5 Conclusions**

The new long term alkenone ε_p records from the Oligocene to early Miocene at North Atlantic Site IODP 1406 and Southern Ocean Site ODP 1168 reveal a significant 8 to 10 % shift. The new records resolve abrupt 3 % declines from 27 to 24.5 Ma and 24 to 22.5 Ma. The long term trend is comparable with previous lower resolution analysis when they are recalculated with the same methodology.

470 In addition to CO_2 , ε_p may be modified by changes in cellular surface area to volume ratio and growth rate regulated by light, temperature and nutrients. However, our assessment of these effects using records of coccolith size and alkenone temperature estimates for exact time intervals of ε_p determination, shows that size and temperature effects have a negligible impact in the long term declining trend. The similarity of ε_p in widely separated sites experiencing contrasting temperature histories strongly suggests a global CO_2 decline as the most likely cause of the declining ε_p . At the same time, our high-resolution sampling
475 reveals significant orbital scale variability in ε_p and underscores the potential for aliasing in low resolution records. Higher resolution ε_p time series, and more precise age models on legacy ε_p records to facilitate more confident comparisons of trends among sites, will provide a better characterization of the key long term trends.

Our results highlight the paradox of complex relationships between CO_2 indicators and SST at both the orbital and multi-million year timescales. The higher resolution sampling between 28.7 to 29.7 Ma shows that orbital ε_p maxima do not coincide
480 with orbital minima in ice volume and/or warmer deep ocean temperature. Similarly, through the late Oligocene warming, CO_2 decline contrasts with evidence for Antarctic ice retreat and evidence of stable or warming SST. The transition from late Oligocene to early Miocene, reaching minimum CO_2 around 19 Ma, is coincident with significant cooling only in the Southern Ocean Site 1168, but not the North Atlantic site which may be more affected by changes in ocean heat transport.

Data availability

485 Data presented in this paper is stored at Zenodo public repository (<https://doi.org/10.5281/zenodo.13908062>)



Author contribution

Study was conceived by HMS and PJP. Analysis completed by JG, SRP, RSW and LA. Interpretation by JG and HMS. Writing of original draft by JG and HMS with support of PJP.

490 Competing interests

The contact author has declared that none of the authors has any competing interests.

Acknowledgments

This paper presents data on sediment samples provided by the Ocean Drilling Program (ODP, IODP). We thank Maddie Santos for lab assistance with biogenic Si determinations. We thank Madalina Jaggi for assistance with carbonate stable isotope
495 measurements.

Financial support

This research was funded by the Swiss National Science Foundation Award 200021_182070 to HMS.

References

- Auderset, A., Moretti, S., Taphorn, B., Ebner, P.-R., Kast, E., Wang, X.T., Schiebel, R., Sigman, D.M., Haug, G.H., Martínez-García, A., 2022. Enhanced ocean oxygenation during Cenozoic warm periods. *Nature* 609, 77-82.
- Baczynski, A.A., Polissar, P.J., Juchelka, D., Schwieters, J., Hilkert, A., Summons, R.E., Freeman, K.H., 2018. Picomolar-scale compound-specific isotope analyses. *Rapid Communications in Mass Spectrometry* 32, 730-738.
- Blaauw, M., Christen, J.A., 2011. Flexible paleoclimate age-depth models using an autoregressive gamma process. *Bayesian analysis* 6, 457-474.
- 505 Boller, A.J., Thomas, P.J., Cavanaugh, C.M., Scott, K.M., 2011. Low stable carbon isotope fractionation by coccolithophore RubisCO. *Geochimica et cosmochimica acta* 75, 7200-7207.
- Bolton, C.T., Hernandez-Sanchez, M.T., Fuertes, M.A., Gonzalez-Lemos, S., Abrevaya, L., Mendez-Vicente, A., Flores, J.A., Probert, I., Giosan, L., Johnson, J., Stoll, H.M., 2016. Decrease in coccolithophore calcification and CO₂ since the middle Miocene. *Nat Commun* 7, 10284.
- 510 Bolton, C.T., Stoll, H.M., 2013. Late Miocene threshold response of marine algae to carbon dioxide limitation. *Nature* 500, 558-562.
- Bradshaw, C.D., Langebroek, P.M., Lear, C.H., Lunt, D.J., Coxall, H.K., Sosdian, S.M., de Boer, A.M., 2021. Hydrological impact of Middle Miocene Antarctic ice-free areas coupled to deep ocean temperatures. *Nature Geoscience* 14, 429-436.
- Breitenbach, S.F., Bernasconi, S.M., 2011. Carbon and oxygen isotope analysis of small carbonate samples (20 to 100 µg) with a GasBench II preparation device. *Rapid Communications in Mass Spectrometry* 25, 1910-1914.
- 515 Consortium, C.P., 2023. Toward a Cenozoic history of atmospheric CO₂. *Science* 382, eadi5177.
- Cramer, B., Miller, K., Barrett, P., Wright, J., 2011. Late Cretaceous–Neogene trends in deep ocean temperature and continental ice volume: Reconciling records of benthic foraminiferal geochemistry (δ¹⁸O and Mg/Ca) with sea level history. *Journal of Geophysical Research: Oceans* 116.
- 520 Curry, W., Shackleton, N., Richter, C., 1995. Leg 154. Synthesis. *Proceedings ODP, Initial Reports* 154, 421-442.
- Deconto, R.M., Pollard, D., Wilson, P.A., Palike, H., Lear, C.H., Pagani, M., 2008. Thresholds for Cenozoic bipolar glaciation. *Nature* 455, 652-656.
- Erdei, B., Utescher, T., Hably, L., Tamas, J., Roth-Nebelsick, A., Grein, M., 2012. Early Oligocene continental climate of the Palaeogene Basin (Hungary and Slovenia) and the surrounding area. *Turkish Journal of Earth Sciences* 21, 153-186.
- 525 Evans, D., Brugger, J., Inglis, G.N., Valdes, P., 2024. The Temperature of the Deep Ocean Is a Robust Proxy for Global Mean Surface Temperature During the Cenozoic. *Paleoceanography and Paleoclimatology* 39, e2023PA004788.
- Exon, N., Kennett, J., Malone, M., 2001. I. LEG 189 SUMMARY, *Proceedings of the Ocean Drilling Program*.
- Foster, G.L., Royer, D.L., Lunt, D.J., 2017. Future climate forcing potentially without precedent in the last 420 million years. *Nature Communications* 8, 14845.
- 530 Freeman, K.H., Hayes, J., 1992. Fractionation of carbon isotopes by phytoplankton and estimates of ancient CO₂ levels. *Global Biogeochemical Cycles* 6, 185-198.
- Golledge, N.R., 2020. Long-term projections of sea-level rise from ice sheets. *Wiley Interdisciplinary Reviews: Climate Change* 11, e634.



- González-Lanchas, A., Hernández-Almeida, I., Flores, J.A., Sierro, F.J., Guitián, J., Stoll, H.M., 2021. Carbon Isotopic Fractionation of Alkenones and Gephyrocapsa Coccoliths Over the Late Quaternary (Marine Isotope Stages 12–9) Glacial-Interglacial Cycles at the Western Tropical Atlantic. *Paleoceanography and Paleoclimatology* 36, e2020PA004175.
- Gradstein, F.M., Ogg, J.G., Schmitz, M., Ogg, G., 2012. The geologic time scale 2012. elsevier.
- Greenop, R., Sosdian, S.M., Henehan, M.J., Wilson, P.A., Lear, C.H., Foster, G.L., 2019. Orbital forcing, ice-volume and CO₂ across the Oligocene-Miocene Transition. *Paleoceanography and Paleoclimatology*.
- 540 Guitián, J., Dunkley Jones, T., Hernández-Almeida, I., Löffel, T., Stoll, H.M., 2020. Adaptations of coccolithophore size to selective pressures during the Oligocene to Early Miocene high CO₂ world. *Paleoceanography and Paleoclimatology* 35, e2020PA003918.
- Guitián, J., Phelps, S., Polissar, P.J., Ausín, B., Eglinton, T.I., Stoll, H.M., 2019. Midlatitude Temperature Variations in the Oligocene to Early Miocene. *Paleoceanography and Paleoclimatology* 34, 1328-1343.
- 545 Guitián, J., Stoll, H.M., 2021. Evolution of Sea Surface Temperature in the Southern Mid-latitudes from Late Oligocene through Early Miocene. *Paleoceanography and Paleoclimatology* 36, e2020PA004199.
- Hansen, J., Sato, M., Russell, G., Kharecha, P., 2013. Climate sensitivity, sea level and atmospheric carbon dioxide. *Philosophical Transactions of the Royal Society A: Mathematical, Physical and Engineering Sciences* 371, 20120294.
- Henderiks, J., Pagani, M., 2007. Refining ancient carbon dioxide estimates: Significance of coccolithophore cell size for alkenone-based pCO₂ records. *Paleoceanography* 22.
- 550 Henderiks, J., Pagani, M., 2008. Coccolithophore cell size and the Paleogene decline in atmospheric CO₂. *Earth and planetary science letters* 269, 576-584.
- Hernández-Almeida, I., Guitián, J., Tanner, T., Zhang, H., Stoll, H.M., 2023. Hydrographic control on carbon isotope fractionation in coccolithophores in the North Atlantic during the Mid-Pleistocene. *Quaternary Science Reviews* 309, 108081.
- 555 Hernández-Almeida, I., Krumhardt, K.M., Zhang, H., Stoll, H.M., 2020. Estimation of physiological factors controlling carbon isotope fractionation in coccolithophores in photic zone and core-top samples. *Geochemistry, Geophysics, Geosystems* 21, e2020GC009272.
- Jasper, J.P., Hayes, J., 1994. Reconstruction of Paleoeceanic PCO₂ levels from carbon isotopic compositions of sedimentary biogenic components, *Carbon Cycling in the Glacial Ocean: Constraints on the Ocean's Role in Global Change*. Springer, pp. 323-341.
- 560 Krumhardt, K.M., Lovenduski, N.S., Iglesias-Rodriguez, M.D., Kleypas, J.A., 2017. Coccolithophore growth and calcification in a changing ocean. *Progress in oceanography* 159, 276-295.
- LaRiviere, J.P., Ravelo, A.C., Crimmins, A., Dekens, P.S., Ford, H.L., Lyle, M., Wara, M.W., 2012. Late Miocene decoupling of oceanic warmth and atmospheric carbon dioxide forcing. *Nature* 486, 97-100.
- 565 Lear, C.H., Elderfield, H., Wilson, P., 2000. Cenozoic deep-sea temperatures and global ice volumes from Mg/Ca in benthic foraminiferal calcite. *science* 287, 269-272.
- Lear, C.H., Rosenthal, Y., Coxall, H.K., Wilson, P., 2004. Late Eocene to early Miocene ice sheet dynamics and the global carbon cycle. *Paleoceanography* 19.
- Levy, R., Meyers, S., Naish, T., Gollledge, N., McKay, R., Crampton, J., DeConto, R., De Santis, L., Florindo, F., Gasson, E., 2019. Antarctic ice-sheet sensitivity to obliquity forcing enhanced through ocean connections. *Nature Geoscience*, 1.
- 570 Liang, J.-Q., Leng, Q., Höfig, D.F., Niu, G., Wang, L., Royer, D.L., Burke, K., Xiao, L., Zhang, Y.G., Yang, H., 2022a. Constraining conifer physiological parameters in leaf gas-exchange models for ancient CO₂ reconstruction. *Global and Planetary Change* 209, 103737.
- Liang, J.-q., Leng, Q., Xiao, L., Höfig, D.F., Royer, D.L., Zhang, Y.G., Yang, H., 2022b. Early Miocene redwood fossils from Inner Mongolia: CO₂ reconstructions and paleoclimate effects of a low Mongolian plateau. *Review of Palaeobotany and Palynology* 305, 104743.
- 575 Liebrand, D., de Bakker, A.T., Beddow, H.M., Wilson, P.A., Bohaty, S.M., Ruessink, G., Palike, H., Batenburg, S.J., Hilgen, F.J., Hodell, D.A., Huck, C.E., Kroon, D., Raffi, I., Saes, M.J., van Dijk, A.E., Lourens, L.J., 2017. Evolution of the early Antarctic ice ages. *Proc Natl Acad Sci U S A* 114, 3867-3872.
- 580 Lisiecki, L.E., Raymo, M.E., 2005. A Pliocene-Pleistocene stack of 57 globally distributed benthic $\delta^{18}O$ records. *Paleoceanography* 20.
- Liu, Z., He, Y., Jiang, Y., Wang, H., Liu, W., Bohaty, S.M., Wilson, P.A., 2018. Transient temperature asymmetry between hemispheres in the Palaeogene Atlantic Ocean. *Nature Geoscience* 11, 656.
- Liu, Z., Pagani, M., Zinniker, D., Deconto, R., Huber, M., Brinkhuis, H., Shah, S.R., Leckie, R.M., Pearson, A., 2009. Global cooling during the eocene-oligocene climate transition. *Science* 323, 1187-1190.
- 585 Londoño, L., Royer, D.L., Jaramillo, C., Escobar, J., Foster, D.A., Cárdenas-Rozo, A.L., Wood, A., 2018. Early Miocene CO₂ estimates from a Neotropical fossil leaf assemblage exceed 400 ppm. *American Journal of Botany* 105, 1929-1937.
- Miller, K.G., Browning, J.V., Schmelz, W.J., Kopp, R.E., Mountain, G.S., Wright, J.D., 2020. Cenozoic sea-level and cryospheric evolution from deep-sea geochemical and continental margin records. *Science advances* 6, eaaz1346.
- 590 Miller, K.G., Wright, J.D., Fairbanks, R.G., 1991. Unlocking the ice house: Oligocene-Miocene oxygen isotopes, eustasy, and margin erosion. *Journal of Geophysical Research: Solid Earth* 96, 6829-6848.
- Misra, S., Froelich, P.N., 2012. Lithium isotope history of Cenozoic seawater: changes in silicate weathering and reverse weathering. *Science* 335, 818-823.
- 595 Mook, W., Bommerson, J., Staverman, W., 1974. Carbon isotope fractionation between dissolved bicarbonate and gaseous carbon dioxide. *Earth and Planetary science letters* 22, 169-176.
- Moraweck, K., Grein, M., Konrad, W., Kvaček, J., Kova-Eder, J., Neinhuis, C., Traiser, C., Kunzmann, L., 2019. Leaf traits of long-ranging Paleogene species and their relationship with depositional facies, climate and atmospheric CO₂ level; Leaf



- traits of long-ranging Paleogene species and their relationship with depositional facies, climate and atmospheric CO₂ level. *Palaeontographica Abteilung B: Palaeophytologie* 298, 93-172.
- 600 Novak, J., McGrath, S.M., Wang, K.J., Liao, S., Clemens, S.C., Kuhnt, W., Huang, Y., 2022. U38MEK' Expands the linear dynamic range of the alkenone sea surface temperature proxy. *Geochimica et Cosmochimica Acta* 328, 207-220.
- O'Brien, C.L., Huber, M., Thomas, E., Pagani, M., Super, J.R., Elder, L.E., Hull, P.M., 2020. The enigma of Oligocene climate and global surface temperature evolution. *Proceedings of the National Academy of Sciences* 117, 25302-25309.
- 605 Pagani, M., Arthur, M.A., Freeman, K.H., 1999. Miocene evolution of atmospheric carbon dioxide. *Paleoceanography* 14, 273-292.
- Pagani, M., Arthur, M.A., Freeman, K.H., 2000. Variations in Miocene phytoplankton growth rates in the southwest Atlantic: Evidence for changes in ocean circulation. *Paleoceanography* 15, 486-496.
- Pagani, M., Holland, H., Turekian, K., 2014. 12.13 Biomarker-based inferences of past climate: The alkenone pCO₂ proxy. *Treatise on Geochemistry*, edited by: Holland, HD and Turekian, KK, Elsevier, Oxford, 361-378.
- 610 Pagani, M., Huber, M., Liu, Z., Bohaty, S.M., Henderiks, J., Sijp, W., Krishnan, S., DeConto, R.M., 2011. The role of carbon dioxide during the onset of Antarctic glaciation. *science* 334, 1261-1264.
- Pagani, M., Zachos, J.C., Freeman, K.H., Tiplle, B., Bohaty, S., 2005. Marked decline in atmospheric carbon dioxide concentrations during the Paleogene. *Science* 309, 600-603.
- Pfuhl, H.A., McCave, I.N., 2003. Integrated age models for the early Oligocene-early Miocene, sites 1168 and 1170-1172. *Proc. ODP, Sci. Results*, pp. 1-21.
- 615 Popp, B.N., Kenig, F., Wakeham, S.G., Laws, E.A., Bidigare, R.R., 1998. Does growth rate affect ketone unsaturation and intracellular carbon isotopic variability in *Emiliana huxleyi*? *Paleoceanography* 13, 35-41.
- Rae, J.W., Zhang, Y.G., Liu, X., Foster, G.L., Stoll, H.M., Whiteford, R.D., 2021. Atmospheric CO₂ over the past 66 million years from marine archives. *Annual Review of Earth and Planetary Sciences* 49, 609-641.
- 620 Ragueneau, O., Tréguer, P., Leynaert, A., Anderson, R., Brzezinski, M., DeMaster, D., Dugdale, R., Dymond, J., Fischer, G., Francois, R., 2000. A review of the Si cycle in the modern ocean: recent progress and missing gaps in the application of biogenic opal as a paleoproductivity proxy. *Global and Planetary Change* 26, 317-365.
- Rama-Corredor, O., Cortina, A., Martrat, B., Lopez, J.F., Grimalt, J.O., 2018. Removal of bias in C37 alkenone-based sea surface temperature measurements by high-performance liquid chromatography fractionation. *Journal of Chromatography A* 1567, 90-98.
- 625 Rau, G., Riebesell, U., Wolf-Gladrow, D., 1997. CO₂aq-dependent photosynthetic 13C fractionation in the ocean: A model versus measurements. *Global Biogeochemical Cycles* 11, 267-278.
- Rau, G.H., Riebesell, U., Wolf-Gladrow, D., 1996. A model of photosynthetic 13C fractionation by marine phytoplankton based on diffusive molecular CO₂ uptake. *Marine Ecology Progress Series* 133, 275-285.
- 630 Raymo, M.E., Ruddiman, W.F., 1992. Tectonic forcing of late Cenozoic climate. *Nature* 359, 117-122.
- Reichgelt, T., D'Andrea, W.J., Valdivia-McCarthy, A.d.C., Fox, B.R., Bannister, J.M., Conran, J.G., Lee, W.G., Lee, D.E., 2020. Elevated CO₂, increased leaf-level productivity, and water-use efficiency during the early Miocene. *Climate of the Past* 16, 1509-1521.
- Reilly, T.J., Miller, K.G., Feigenson, M.D., 2002. Latest Eocene-earliest Miocene Sr isotopic reference section, Site 522, eastern South Atlantic. *Paleoceanography* 17, 18-11-18-19.
- 635 Roth-Nebelsick, A., Oehm, C., Grein, C., Kunzmann, L., Friedrich, J.-P., Konrad, W., 2014. Stomatal density and index data of *Platanus neptuni* leaf fossils and their evaluation as a CO₂ proxy for the Oligocene. *Review of Palaeobotany and Palynology* 206, 1-9.
- Rugenstein, J.K.C., Ibarra, D.E., von Blanckenburg, F., 2019. Neogene cooling driven by land surface reactivity rather than increased weathering fluxes. *Nature* 571, 99-102.
- 640 Salabarnada, A., Escutia, C., Röhl, U., Nelson, C.H., McKay, R., Jiménez-Espejo, F., Bijl, P., Hartman, J., Strother, S., Salzmann, U., 2018. Paleoceanography and ice sheet variability offshore Wilkes Land, Antarctica—Part 1: Insights from late Oligocene astronomically paced contourite sedimentation. *Climate of the Past* 14, 991-1014.
- Shackleton, N., 1987. Oxygen isotopes, ice volume and sea level. *Quaternary science reviews* 6, 183-190.
- 645 Soslidan, S.M., Greenop, R., Hain, M., Foster, G.L., Pearson, P.N., Lear, C.H., 2018. Constraining the evolution of Neogene ocean carbonate chemistry using the boron isotope pH proxy. *Earth and Planetary Science Letters* 498, 362-376.
- Steinthorsdottir, M., Jardine, P.E., Rember, W.C., 2021. Near-future pCO₂ during the hot Mid Miocene Climatic Optimum. *Paleoceanography and Paleoclimatology* 36.
- 650 Stoll, H.M., Guitian, J., Hernandez-Almeida, I., Mejia, L.M., Phelps, S., Polissar, P., Rosenthal, Y., Zhang, H., Ziveri, P., 2019. Upregulation of phytoplankton carbon concentrating mechanisms during low CO₂ glacial periods and implications for the phytoplankton pCO₂ proxy. *Quaternary Science Reviews* 208, 1-20.
- Stoll, H.M., Pena, L.D., Hernandez-Almeida, I., Guitián, J., Tanner, T., Pälke, H., 2024. Nonlinear increase in seawater ⁸⁷Sr/⁸⁶Sr in the Oligocene to early Miocene and implications for climate-sensitive weathering. *Clim. Past* 20, 25-36.
- 655 Sun, B.-N., Wang, Q.-J., Konrad, W., Ma, F.-J., Dong, J.-L., Wang, Z.-X., 2017. Reconstruction of atmospheric CO₂ during the Oligocene based on leaf fossils from the Ningming Formation in Guangxi, China. *Palaeogeography, Palaeoclimatology, Palaeoecology* 467, 5-15.
- Super, J.R., Thomas, E., Pagani, M., Huber, M., O'Brien, C., Hull, P.M., 2018. North Atlantic temperature and p CO₂ coupling in the early-middle Miocene. *Geology* 46, 519-522.
- 660 Sutton, R.T., Dong, B., Gregory, J.M., 2007. Land/sea warming ratio in response to climate change: IPCC AR4 model results and comparison with observations. *Geophysical research letters* 34.



- Tanner, T., Hernández-Almeida, I., Drury, A.J., Guitián, J., Stoll, H., 2020. Decreasing atmospheric CO₂ during the late Miocene cooling. *Paleoceanography and Paleoclimatology* 35, e2020PA003925.
- Tesfamichael, T., Jacobs, B., Tabor, N., Michel, L., Currano, E., Feseha, M., Barclay, R., Kappelman, J., Schmitz, M., 2017. Settling the issue of “decoupling” between atmospheric carbon dioxide and global temperature: [CO₂] atm reconstructions across the warming Paleogene-Neogene divide. *Geology* 45, 999-1002.
- 665 Tierney, J.E., Tingley, M.P., 2015. A TEX(8)(6) surface sediment database and extended Bayesian calibration. *Sci Data* 2, 150029.
- Tierney, J.E., Tingley, M.P., 2018. BAYSPLINE: A new calibration for the alkenone paleothermometer. *Paleoceanography and Paleoclimatology* 33, 281-301.
- 670 Torres Romero, I., Clark, A.J., Wijkker, R.S., Jaggi, M., Zhang, H., Stoll, H.M., 2024. Temperature-dependent carbon isotope fractionation in coccolithophores. *Frontiers in Earth Science* 12, 1331179.
- Torsvik, T.H., Van der Voo, R., Preeden, U., Mac Niocaill, C., Steinberger, B., Doubrovine, P.V., Van Hinsbergen, D.J., Domeier, M., Gaina, C., Tohver, E., 2012. Phanerozoic polar wander, palaeogeography and dynamics. *Earth-Science Reviews* 114, 325-368.
- 675 van Hinsbergen, D.J., de Groot, L.V., van Schaik, S.J., Spakman, W., Bijl, P.K., Sluijs, A., Langereis, C.G., Brinkhuis, H., 2015. A paleolatitude calculator for paleoclimate studies. *PloS one* 10.
- Van Peer, T.E., Xuan, C., Lippert, P.C., Liebrand, D., Agnini, C., Wilson, P.A., 2017. Extracting a detailed magnetostratigraphy from weakly magnetized, Oligocene to early Miocene sediment drifts recovered at IODP Site U1406 (Newfoundland margin, northwest Atlantic Ocean). *Geochemistry, Geophysics, Geosystems* 18, 3910-3928.
- 680 Westerhold, T., Marwan, N., Drury, A.J., Liebrand, D., Agnini, C., Anagnostou, E., Barnet, J.S., Bohaty, S.M., De Vleeschouwer, D., Florindo, F., 2020. An astronomically dated record of Earth’s climate and its predictability over the last 66 million years. *Science* 369, 1383-1387.
- Wilkes, E.B., Lee, R.B., McClelland, H.L., Rickaby, R.E., Pearson, A., 2018. Carbon isotope ratios of coccolith-associated polysaccharides of *Emiliania huxleyi* as a function of growth rate and CO₂ concentration. *Organic geochemistry* 119, 1-10.
- 685 Zachos, J., Pagani, M., Sloan, L., Thomas, E., Billups, K., 2001. Trends, rhythms, and aberrations in global climate 65 Ma to present. *Science* 292, 686-693.
- Zachos, J.C., Dickens, G.R., Zeebe, R.E., 2008. An early Cenozoic perspective on greenhouse warming and carbon-cycle dynamics. *Nature* 451, 279-283.
- 690 Zhang, Y.G., Pagani, M., Liu, Z., Bohaty, S.M., Deconto, R., 2013. A 40-million-year history of atmospheric CO₂. *Philos Trans A Math Phys Eng Sci* 371, 20130096.